PNAS NEXUS

PNAS Nexus, 2025, 4, pgaf085

https://doi.org/10.1093/pnasnexus/pgaf085
Advance access publication 18 March 2025
Research Report

Clinical and molecular landscape of prolonged SARS-CoV-2 infection with resistance to remdesivir in immunocompromised patients

Chisako Iriyama[a,1], Takaya Ichikawa[b,c,d,1], Tomokazu Tamura[b,e,f], Mutsumi Takahata[g], Takashi Ishio[g], Makoto Ibata[g], Ryuji Kawai[h], Mitsunaga Iwata[h], Masahiro Suzuki[i], Hirokazu Adachi[j], Naganori Nao[f,k], Hikoyu Suzuki[l], Akito Kawai[i], Akifumi Kamiyama[b], Tadaki Suzuki[m], Yuichiro Hirata[m], Shun Iida[m], Harutaka Katano[m], Yasushi Ishii[n], Takahiro Tsuji[n], Yoshitaka Oda[o], Shinya Tanaka[o,p], Nanase Okazaki[n], Yuko Katayama[n], Shimpei Nakagawa[n], Tetsuya Tsukamoto[q], Yohei Doi[i,r,s,t], Takasuke Fukuhara[b,e,f,u,v,*,2], Takayuki Murata[r,w] and Akihiro Tomita[a,*]

[a]Department of Hematology, Fujita Health University School of Medicine, 1-98 Dengakugakubo, Kutsukake-cho, Toyoake 470-1192, Japan
[b]Department of Microbiology and Immunology, Faculty of Medicine, Hokkaido University, N15 W7, Kita-ku, Sapporo 060-8638, Japan
[c]Department of Hematology, Faculty of Medicine, Hokkaido University, Sapporo 060-8638, Japan
[d]Department of Hematology, Sapporo City General Hospital, Sapporo 060-8604, Japan
[e]Institute for Vaccine Research and Development (IVReD), Hokkaido University, Sapporo 001-0021, Japan
[f]One Health Research Center, Hokkaido University, Sapporo 060-0818, Japan
[g]Department of Hematology, Sapporo-Kosei General Hospital, Sapporo 060-0033, Japan
[h]Department of Emergency and General Internal Medicine, Fujita Health University School of Medicine, Toyoake 470-1192, Japan
[i]Department of Microbiology, Fujita Health University School of Medicine, Toyoake 470-1192, Japan
[j]Department of Microbiology and Medical Zoology, Aichi Prefectural Institute of Public Health, Nagoya 462-8576, Japan
[k]Division of International Research Promotion, International Institute for Zoonosis Control, Hokkaido University, Sapporo 001-0020, Japan
[l]Digzyme Inc., Tokyo 105-0004, Japan
[m]Department of Pathology, National Institute of Infectious Diseases, Tokyo 162-8640, Japan
[n]Department of Pathology, Sapporo City General Hospital, Sapporo 060-8604, Japan
[o]Department of Cancer Pathology, Faculty of Medicine, Hokkaido University, Sapporo 060-8638, Japan
[p]Institute for Chemical Reaction Design and Discovery (WPI-ICReDD), Hokkaido University, Sapporo 001-0021, Japan
[q]Department of Diagnostic Pathology, Fujita Health University School of Medicine, Toyoake 470-1192, Japan
[r]Center for Infectious Disease Research, Fujita Health University, Toyoake 470-1192, Japan
[s]Department of Infectious Diseases, Fujita Health University School of Medicine, Toyoake 470-1192, Japan
[t]Division of Infectious Diseases, University of Pittsburgh School of Medicine, Pittsburgh, PA 15261, USA
[u]Laboratory of Virus Control, Research Institute for Microbial Diseases, Osaka University, Suita 565-0871, Japan
[v]AMED-CREST, Japan Agency for Medical Research and Development (AMED), Tokyo 100-0004, Japan
[w]Department of Virology, Fujita Health University School of Medicine, Toyoake 470-1192, Japan
*To whom correspondence should be addressed: Email: atomita@fujita-hu.ac.jp (A.T.); Email: fukuhara.takasuke.169@m.kyushu-u.ac.jp (T.F.)
[1]C.I. and T.I. contributed equally to this work.
[2]Present address: Department of Virology, Faculty of Medical Sciences, Kyushu University, Fukuoka 812-8582, Japan.
Edited By Richard Stanton

Abstract

Patients with hematologic diseases have experienced coronavirus disease 2019 (COVID-19) with a prolonged, progressive course. Here, we present clinical, pathological, and virological analyses of three cases of prolonged COVID-19 among patients undergoing treatment for B-cell lymphoma. These patients had all been treated with anti-CD20 antibody and bendamustine. Despite various antiviral treatments, high severe acute respiratory syndrome coronavirus 2 (SARS-CoV-2) levels persisted for >4 weeks, and two of them succumbed to COVID-19. The autopsy showed bronchopneumonia, interstitial pneumonia, alveolar hemorrhage, and fibrosis. Overlapping cytomegalovirus, fungal and/or bacterial infections were also confirmed. Sequencing of SARS-CoV-2 showed accumulation of mutations and changes in variant allele frequencies over time. NSP12 mutations V792I and M794I appeared independently in two cases as COVID-19 progressed.

Competing Interest: N.N.: employment; Fasmac Co., Ltd. Y.D.: consultancy within the past 2 years; GSK, Moderna, Gilead Sciences, Shionogi, Meiji Seika, Pfizer, AbbVie, research funding; Entasis. M.S.: honoraria received directly from an entity; Kanto Chemical Co. Inc., any other potential financial relationship; Kanto Chemical Co. Inc. A.T.: research funding; Chugai Pharmaceutical, Astellas Pharma, Eisai, Otsuka Pharmaceutical, Ono Pharmaceutical, Kyowa Kirin, Shionogi, Sumitomo Dainippon Pharma, Taiho Pharmaceutical, Takeda Pharmaceutical, Teijin, Nippon Shinyaku, Nihon Pharmaceutical, Pfizer Japan, Mochida Pharmaceutical, Yakult Honsha, and Perseus Proteomics, and received lecture fee from AstraZeneca, Chugai Pharmaceutical, AbbVie GK, Genmab, Ono Pharmaceutical, Kyowa Kirin, Eisai, Takeda Pharmaceutical, Astellas Pharma, Nippon Shinyaku, Janssen Pharmaceutical, Zenyaku Kogyo, Bristol-Myers Squibb, and SymBio Pharmaceutical. C.I., T.Ic., T.Ta., M.T., T.Is., M.Ib., R.K. M.Iw., H.A., H.S., A.Kaw., A.Kam., T.S., Y.H., S.I., H.K., Y.I., T.Ts., Y.O., S.T., N.O., Y.K., S.N., T.Tsuk., T.F., and T.M. have nothing to disclose.

Received: June 17, 2024. **Accepted:** February 15, 2025

In vitro drug susceptibility analysis and an animal experiment using recombinant SARS-CoV-2 demonstrated that each mutation, V792 and M794I, was independently responsible for remdesivir resistance and attenuated pathogenicity. E340A, E340D, and F342INS mutations in the spike protein were found in one case, which may account for the sotrovimab resistance. Analysis of autopsy specimens indicated heterogeneous distribution of these mutations. In summary, we demonstrated temporal and spatial diversity in SARS-CoV-2 that evolved resistance to various antiviral agents in malignant lymphoma patients under immunodeficient conditions caused by certain types of immunochemotherapies. Strategies may be necessary to prevent the acquisition of drug resistance and improve outcomes, such as the selection of appropriate treatment strategies for lymphoma considering patients' immune status and the institution of early intensive antiviral therapy.

Keywords: malignant lymphoma, SARS-CoV-2, COVID-19, remdesivir, drug resistance

Significance Statement

In immunocompromised patients with hematological malignancies, prolonged/progressive course of Coronavirus disease 2019 (COVID-19) is still a critical problem, even in an era when vaccines and several antiviral therapeutics have been developed. Here, we analyzed serial viral specimens of three B-cell lymphoma patients undergoing immunochemotherapies who experienced prolonged/progressive course of COVID-19 and demonstrated that diverse genetic mutations on severe acute respiratory syndrome coronavirus 2 (SARS-CoV-2) accumulated on therapy within each individual. In vitro drug susceptibility assay revealed that specific genetic alterations on NSP12 (V792I and M794I) were responsible for the acquisition of remdesivir resistance. These findings indicate that mutations related to drug resistance accumulate in SARS-CoV-2 in immunocompromised patients, suggesting the importance of treatment strategies that can eradicate the virus at an early stage of COVID-19 onset.

Introduction

Coronavirus disease 2019 (COVID-19), caused by severe acute respiratory syndrome coronavirus 2 (SARS-CoV-2), is a life-threatening infection among patients with underlying diseases and advanced age (1). Prolonged infection and severe disease have been reported in patients with hematologic malignancies (2–4). Higher rates of severe disease have also been noted, especially in patients with lymphoid malignancies undergoing certain immunochemotherapy regimens and cell therapies, including chimeric-antigen-receptor T-cell therapy, suggesting that humoral and cellular immune deficiency may be closely associated with negative outcomes of COVID-19 (5).

Since the onset of the pandemic, the prognosis of COVID-19 has gradually improved with the use of monoclonal antibody therapeutics sotrovimab (6), casirivimab/imdevimab (7), and tixagevimab/cilgavimab (8); antiviral drugs remdesivir (9), molnupiravir (10), and ritonavir-boosted nirmatrelvir (11); and anti-SARS-CoV-2 mRNA vaccines (12, 13). However, subtypes of SARS-CoV-2, such as BA.2-BA.5, XBB, and BQ.1, have emerged as a result of immune escape (14–18). These viruses have many additional mutations, mainly in the receptor-binding domain (RBD) of the spike protein (19), and demonstrate various degrees of resistance to antibody therapeutics and monovalent/bivalent vaccines (14–18). The emergence of remdesivir resistance through mutations in NSP12 in ORF1b (20), which encodes an RNA-dependent polymerase (RdRp), has been reported (21), but small-molecule antiviral agents, including remdesivir, have generally maintained their activity throughout the pandemic (16, 17). In addition, insufficient antibody acquisition after vaccination has been reported in patients vaccinated <1 year after the last administration of immunochemotherapy, including the anti-CD20 antibody rituximab and obinutuzumab, and in patients using Bruton's tyrosine kinase (BTK) inhibitors and Janus kinase 2 inhibitors (22, 23).

Against these backgrounds, COVID-19 remains a life-threatening infection among patients with hematologic malignancies, even as the public threat of SARS-CoV-2 has been waning overall. These patients may still suffer from refractory diseases after the clinical signs of COVID-19 have subsided, with persistence of high viral copy numbers after infection, emergence of resistance to various antiviral therapies, and chronic clinical course leading to worsening pneumonia and other complications leading to death.

In the present study, we analyzed three cases of prolonged COVID-19 from clinical, histopathological, and molecular biological aspects. Longitudinal analysis of the viral genome detected genetic mutations associated with remdesivir and sotrovimab resistance, which showed temporal and spatial diversity. These findings provide important insights into the management of COVID-19 in patients with hematologic diseases.

Methods

Patients' characteristics

Three patients with B-cell lymphoma (BCL) who developed COVID-19 between January and December in 2022, had persistent SARS-CoV-2 infection for >8 weeks despite antiviral treatment, and whose nasal swab specimens were stored over time were included from three hospitals in Japan. Omicron strains (BA.1.1, BA.2, and BA.5) were prevalent during this period encompassing the sixth and seventh waves in Japan. All patients were being treated with bendamustine and an anti-CD20 antibody. The use of clinical information and residual samples was approved by the Ethical Review Committee of each institution (Fujita Health University: HM21-067, HM21-179, and HM23-016; Sapporo City General Hospital: R-04-063-951, Sapporo Kosei Hospital: 621). Written consent was obtained from each patient, and the specimens obtained from the patients were de-identified for further study.

Detection of SARS-CoV-2

SARS-CoV-2 was detected qualitatively by antigen testing or PCR using nasal swabs. For patients with hematological diseases, including BCL, quantitative reverse transcription-PCR (qRT-PCR) was also performed in the clinical laboratory upon request as part of routine clinical care, where viral RNA was extracted from the viral culture medium of the swab samples and subjected to copy number analysis or cycle threshold (Ct) value analysis. Detailed strategies are indicated in Supplementary Methods.

Pathological analyses

Autopsies were performed for cases 1 and 2 within 6 h of the patients' death. Detailed information is indicated in Supplementary Methods.

Mutational analyses of SARS-CoV-2

Case 1: Genome sequencing of SARS-CoV-2 was performed according to the protocol of the National Institute of Infectious Diseases (https://www.protocols.io/view/ncov-2019-sequencing-protocol-for-illumina-eq2ly398mgx9/v5) using MiSeq (for swab) or NextSeq 1000 (for autopsy; Illumina, San Diego, CA). Obtained sequences were mapped to the reference sequence (SARS-CoV-2 Wuhan strain, MN908947.3). Detailed information is depicted in Supplementary Methods.

Cases 2 and 3: Sangar sequencing using SeqStudio Genetic Analyzer (Thermo Fisher Scientific) was performed to determine the whole viral genome sequence, as previously reported (24). Detailed information is indicated in Supplementary Methods.

Rescue of the recombinant viruses

The recombinant viruses with remdesivir resistance mutations and/or the GFP gene were rescued by the CPER method, which was established previously (25). V792I or M794I in NSP12 was individually introduced into the viral genome fragment-cloning plasmid by inverse PCR and in-fusion reaction using an In-Fusion Snap Assembly Master Mix (Takara Bio). A GFP gene was introduced as a replacement for the ORF7a region, as previously described (26). Sanger sequencing (Fig. S1) and comprehensive next-generation sequencing analyses (data not shown) using stock viruses verified that each point mutation was correctly introduced. The detailed procedure is indicated in Supplementary Methods.

In vitro drug susceptibility testing and growth kinetics assay

VeroE6/TMPRSS2 cells (VeroE6 cells stably expressing human TMPRSS2 (27)), HEK293-ACE2/TMPRSS2 cells (HEK293 cells stably expressing human ACE2 and TMPRSS2 (28)), and Vero cells were utilized for in vitro drug susceptibility testing and growth kinetics assay. Detailed information is indicated in Supplementary Methods.

Results

Clinical courses of patients with resistance to anti-SARS-CoV-2 therapeutics

Case 1

A 65-y-old male with relapsed follicular lymphoma (FL) had received six courses of obinutuzumab and bendamustine (Obi-B) leading to complete remission (CR), which was followed by Obi maintenance (Obi-Mt; Fig. 1A). He had received two doses of SARS-CoV-2 mRNA vaccine during Obi-Mt; however, antispike antibody was not detected. SARS-CoV-2 infection was diagnosed in January 2021, 5 months after obtaining CR. He did not have pneumonia at diagnosis (Fig. 1A, a and e), and was treated with sotrovimab monotherapy and discharged. However, persistent fever resulted in re-admission 2 weeks later. Computed tomography (CT) showed multiple bilateral ground-glass opacities (Fig. 1A, b and f). He was treated with multiple courses of antiviral drugs, including remdesivir, nirmatrelvir-ritonavir, and molnupiravir with or without tocilizumab considering the intensity of the inflammatory status. He also received systemic corticosteroids. However, his oxygenation declined until ventilator management was required (Fig. 1A, c and d). During these treatments, he also suffered from sepsis, cytomegalovirus (CMV) antigenemia, and acute pulmonary aspergillosis. CD4- and CD19-positive cell counts in peripheral blood remained low (Fig. 1A, middle part). The copy numbers of SARS-CoV-2 gradually increased despite intensive treatment (Fig. 1A, purple line). He died of respiratory failure 7 months after onset.

Case 2

A 75-y-old male with head-and-neck diffuse large BCL (DLBCL) had received three courses of R-VP (rituximab, vincristine, and prednisolone) and six courses of Pola-BR (polatuzumab vedotin, bendamustine, and rituximab). The lymphoma did not achieve remission, and he underwent salvage radiation therapy in June 2022. During this hospitalization, he developed COVID-19 due to an in-hospital outbreak. He had received two doses of SARS-CoV-2 mRNA vaccine prior to chemotherapy, and acquisition of antispike antibody was confirmed at the onset, but CD4-positive T-cell counts were critically low (Fig. 1B). His symptoms were sore throat and mild cough. He was treated with combination therapy using sotrovimab and remdesivir given the severe immunodeficiency and discharged 15 days after onset. On day 18, the patient was hospitalized again with bacterial pneumonia: a CT scan showed infiltrates without ground-glass opacities in the right inferior lobe (Fig. 1B, a and b). He was treated with broad-spectrum antibiotics, but subsequently had gastrointestinal perforation with bleeding on day 25 (Fig. 1B, c). Surgery was not indicated due to poor condition, and he died of sepsis on day 34. Ct values for SARS-CoV-2 persisted around 20 during his clinical course.

Case 3

A 75-y-old female with FL had completed six courses of Obi-B and subsequently received Obi-Mt (Fig. 1C) under the status of CR. She had received three doses of SARS-CoV-2 vaccine during chemotherapy, followed by tixagevimab/cilgavimab administration in early December 2022. CD4-positive T-cell counts were critically low. SARS-CoV-2 infection was diagnosed by antigen and PCR testing in late December 2022 when she presented with fatigue, cough, and runny nose. Mild interstitial pneumonia was observed upon diagnosis (Fig. 1C, a). She was treated with dexamethasone and remdesivir and was discharged upon improvement of the symptoms. However, she developed a fever again and was readmitted on day 18. CT scan showed multiple bilateral ground-glass opacities (Fig. 1C, b). She was treated again with remdesivir in addition to baricitinib and dexamethasone/prednisolone, considering her severe inflammatory condition. However, CT scan on day 32 showed persistent pneumonia (Fig. 1C, c). The Ct values for SARS-CoV-2 remained around 20 for ~8 weeks. CT scan on day 66 was consistent with organizing pneumonia in the left lung (Fig. 1C, d). She was eventually discharged on day 73 with home oxygen therapy.

Mutations identified in SARS-CoV-2 during the disease course

Nasal swabs were collected periodically during their clinical course and analyzed for mutations in the SARS-CoV-2 genome using the Wuhan strain as a reference. In case 1, multiple nonsynonymous mutations in the spike protein were detected as the disease progressed (Fig. 1A, lower panel, blue and red boxes). Of these, the E340A substitution has been reported to be critical in sotrovimab resistance (29). An insertion F342INS was also detected in its vicinity, in which F342 was substituted to amino acid sequence LTRMV due to 12-bp insertion. V792I substitution in NSP12 of ORF1b was detected immediately after the first course of remdesivir, and then M794I substitution was also detected during the second

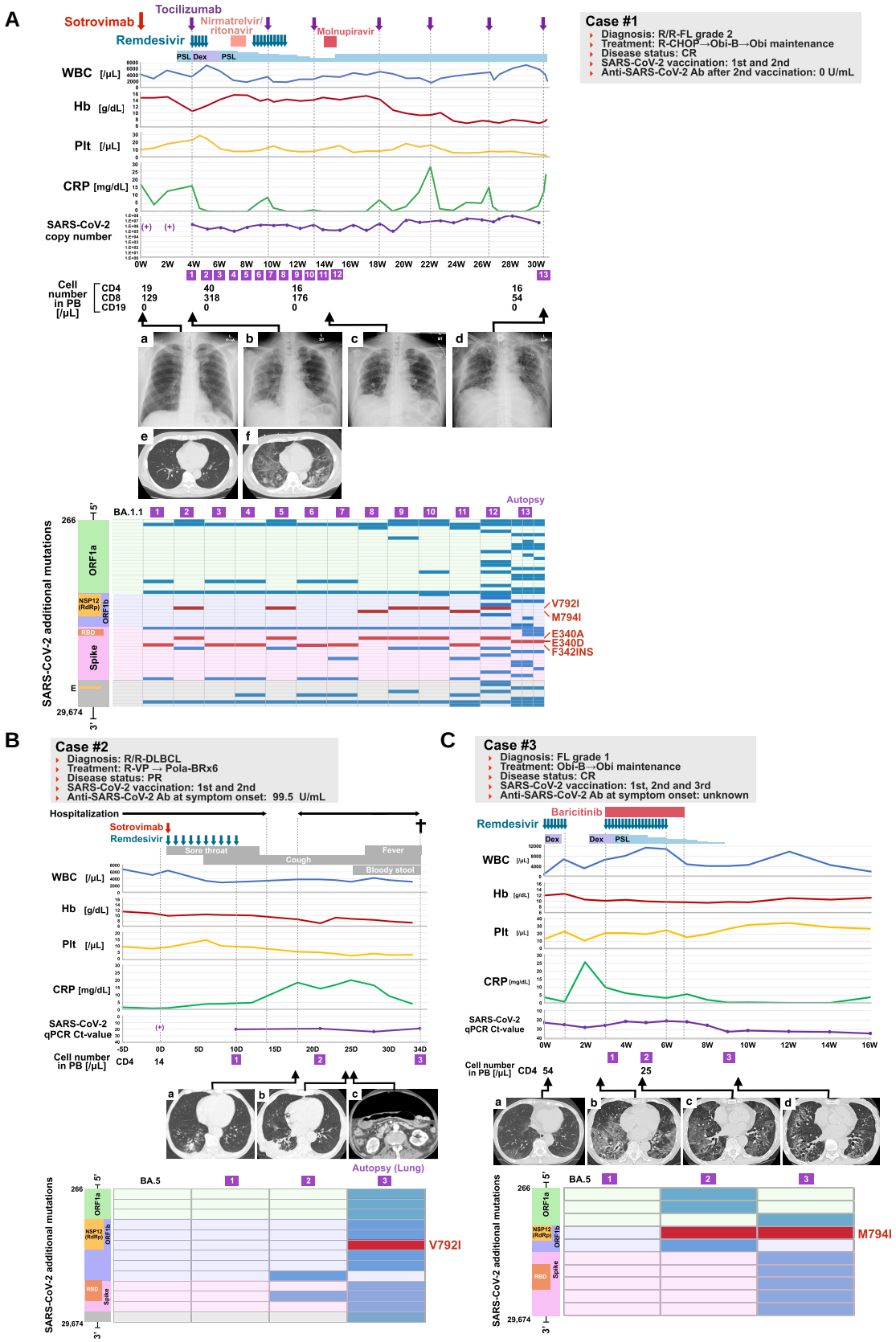

Fig. 1. Clinical courses and SARS-CoV-2 mutation analysis of three cases. On the top panel, the timeline of medications administered is shown with white blood cell count, hemoglobin level, platelet count, CRP, and viral copy number of SARS-CoV-2 since the day of onset (0W in A and C, and 0D in B). The numbers in square boxes are time points when mutation analyses were performed. In the middle panel, chest X-ray and CT scan at each time point are shown (a–f). On the bottom panel, additional mutations that were observed during treatment are shown. Diagram of SARS-CoV-2 coding region is on the left. Darkly painted boxes show acquired mutations. The boxes marked with amino acids (V792I, M794I, E340A, E340D, and F342INS) show mutations implicated in drug resistance. A: case 1, B: case 2, C: case 3. R/R, refractory/relapsed; WBC, white blood cell; Hb, hemoglobin; Plt, platelet; PSL, prednisolone; Dex, dexamethasone; PB, peripheral blood; W, weeks; D, days.

course of remdesivir. Analysis of the lung tissue at autopsy from three different sites confirmed mutations identical with those found between weeks 4 and 16, as well as newly acquired mutations (Fig. 1A, lower panel, sample 13, and Fig. S2). A trend toward the accumulation of additional genetic changes in the terminal stages of the disease was observed as the disease progressed, but the changes were not consistent and diversified over time.

In case 2, three specimens were collected over the course (Fig. 1B, lower panel). Samples obtained 20 days after the start of sotrovimab and remdesivir showed an additional genetic abnormality in the RBD of the spike protein, and samples taken at autopsy showed V792I substitution in NSP12. In this case, a trend toward the accumulation of additional genetic abnormalities was also observed as the disease progressed.

In case 3, three samples were collected over time, and we detected the M794I substitution in NSP12 approximately 30 days after the first course of remdesivir was started. A trend toward the accumulation of additional genetic abnormalities over time was also observed in this case. No anti-SARS-CoV-2 antibody therapeutic agents were used in this case, but samples collected 9 weeks after treatment initiation showed accumulation of genetic changes in the spike protein.

Heterogeneity of additional genetic mutations in SARS-CoV-2 in the airway

Heterogeneity of mutations on SARS-CoV-2 was analyzed using pulmonary tissues from three different areas of the airway (right and left lungs and trachea) of the autopsy specimens (Fig. 1A lower panel and Fig. S2). Mutations were widely distributed in ORF1a, ORF1b, and the S-protein domain. Interestingly, mutation profiles differed among samples, suggesting independent and heterogeneous evolution of the virus within the airway.

Persistent SARS-CoV-2 infection and concomitant infection with CMV

Autopsies were immediately performed following death for cases 1 (Fig. 2A) and 2 (Fig. 2B). For case 1, lung stiffening with acute bronchiolitis, interstitial pneumonia, and alveolar hemorrhage was observed macroscopically (Fig. 2A, a–d). Microscopically, the lung demonstrated acute bronchopneumonia (Fig. 2A, e), diffuse alveolar damage in exudative to proliferative stages (Fig. 2A, g) with squamous metaplasia (Fig. 2A, f), and fibrin thrombi (Fig. 2A, h and i). The lesions involved almost the entire lung. SARS-CoV-2-infected cells (Fig. 2A, j and k) and CMV-infected giant cells with an owl's eye appearance were demonstrated by immunohistochemistry (IHC; Fig. 2A, l and m). A small number of giant cells were positive for both SARS-CoV-2 and CMV, showing clear localization of SARS-CoV-2 in the cytoplasm and CMV in the nucleus, respectively (Fig. 2A, n and o). HHV-6B mRNA was detected by RT-PCR at low copy number (Table S1), but infected cells were not confirmed by IHC (data not shown).

For case 2, the findings of the pneumonia lesions were similar to case 1 (Fig. 2B, a–c). A pneumonia lesion in the right inferior lobe showed "fibrin balls" and hemorrhage within alveolar spaces mixed with organizing fibroblastic tissue without hyaline membrane formation (Fig. 2B, b); these findings were compatible with acute fibrinous and organizing pneumonia (AFOP). Another pneumonia lesion in the right inferior lobe showed aspiration pneumonia (Fig. 2B, c). By IHC, CMV-infected cells and SARS-CoV-2-infected cells were simultaneously observed in both lungs (Fig. 2B, d–g). Of them, CMV-infected cells were found more extensively and predominantly.

In addition, we collected several parts of organs and quantified SARS-CoV-2 RNA (cases 1 and 2) and CMV and HHV-6B DNA (case 1) by qPCR (Table S1). As expected, SARS-CoV-2 RNA was detected in respiratory organs. In case 1, CMV and HHV-6B DNA were also identified, but the latter was in low copy numbers. In case 2, SARS-CoV-2 RNA was undetectable in the heart, liver, spleen, kidneys, and serum, which suggests that systemic infection had not developed (Table S2).

Mutations observed in NSP12 and remdesivir resistance

V792I or M794I, located close to the binding site of remdesivir to NSP12 (Fig. 3A and B), was predominantly selected in all cases (Fig. 1A–C). To determine the role of these two mutations in remdesivir susceptibility and viral replication, we generated recombinant SARS-CoV-2 with each mutation individually based on strain JPN/TY/WK-521 (GISAID ID: EPI_ISL_408667) by using CPER method (25). Sequences of the recombinant viruses were checked by Sanger sequencing (Fig. S1) and next-generation comprehensive analysis, and the mutation introduction rates for V792I and M794I were 97.47 and 97.92%, respectively. We first evaluated remdesivir susceptibility of V792I and M794I mutants using HEK293 cells (28) and Vero cells (27). Because Vero cells express high amounts of P-gp, an ATP-dependent efflux pump with a broad substrate specificity (31), P-gp inhibitor was treated with Vero cells. Both V792I and M794I mutants were less susceptible to remdesivir than the wild-type (WT) virus (Fig. 4A). Compared with WT, the EC_{50} of the V792I/M794I mutants increased 2.97/2.39-fold in HEK293 cells and 4.84/4.30-fold in Vero cells, respectively.

We then examined the in vitro growth efficiency and the in vivo pathogenicity of the two remdesivir-resistant viruses. Growth kinetics using Vero cells in the absence of remdesivir showed that the virus titers of the V792I mutant were lower than those of WT at 12 and 24 h postinfection, and similarly, M794I mutant was slightly slow compared with WT, albeit no significant differences (Fig. 4B, left panel). On the contrary, in the presence of remdesivir (0.1 μM), the virus titers of V792I and M794I mutants were apparently higher than those of WT as expected (Fig. 4B, right panel). In an animal experiment using hamsters, whereas WT infection resulted in marked weight loss, infection with either of the two mutants significantly ameliorated the body weight loss, indicating that the remdesivir-resistant viruses exhibited lower pathogenicity in vivo (Fig. 4C).

To determine the therapeutic effect of remdesivir in the resistant viruses, we further carried out another infection experiment with remdesivir treatment. Hamsters infected with WT, V792I, and M794I mutant viruses were administered remdesivir (15 mg/kg/day) or vehicle control (only WT group) at 0 and 1 dpi (Fig. S4A). Compared with remdesivir treatment and vehicle control in WT groups, hamsters treated with remdesivir exhibit milder weight loss at 1 and 2 dpi, but the weight gaps have disappeared after 3 dpi. The results suggest that the effects of remdesivir were immediately lost within a few days of administration. Comparing with WT and each resistant virus under remdesivir treatment, no differences were observed among the three groups in the early phase of infection. Considering that the virulence of the resistant viruses was attenuated compared with the WT without remdesivir, V792I and M794I showed resistance to remdesivir in vivo as well as in vitro. Viral RNA levels in the lungs at 7 dpi were comparable in any of the groups, both with and without remdesivir (Fig. S4B). Viral RNA levels and viral nucleocapsid protein amount in IHC analysis using lung samples at 2 dpi were also comparable in each group with/without remdesivir (data not shown).

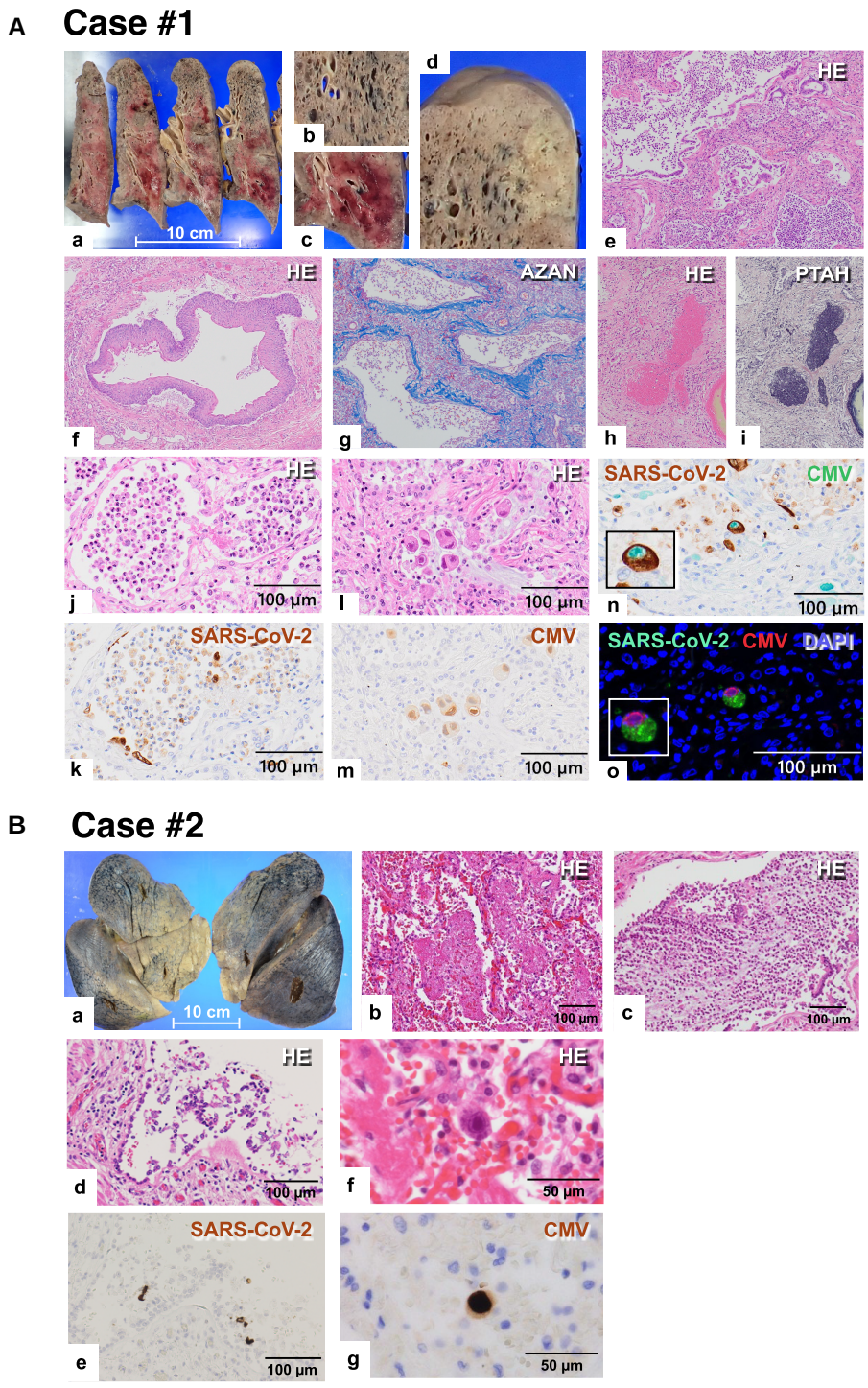

Fig. 2. Pathological observations of the lung lesions at autopsy. A) Autopsy findings of case 1.a–d), gross findings on the lung tissues. b–d) Enlarged view of lesions of interstitial pneumonia (b), pulmonary hemorrhage (c), and bronchopneumonia (d). (e–i) Histological findings of the lungs: bronchopneumonia with neutrophil infiltration (e), squamous metaplasia (f), and interstitial fibrosis (g). h and i) Fibrin thrombi (×100). j and k) SARS-CoV-2-infected cells. l and m) CMV-infected giant cells with an owl's eye appearance. n) Coinfection of SARS-CoV-2 and CMV in the same cell demonstrated by immunostaining. Brown (3,3′-diaminobenzidine) and green (Vina Green) signals indicate SARS-CoV-2 and CMV, respectively. o) Coinfection of SARS-CoV-2 and CMV in the same cell demonstrated by fluorescent staining. Green (Alexa Fluor 488) and red (Alexa Fluor 568) signals indicate SARS-CoV-2 and CMV, respectively. Nuclear labeling was performed using DAPI (blue). B) Autopsy findings of case 2. a) The gross findings on the lung tissues. b and c), histological findings of the AFOP-like lesion (b) and the consolidation lesion (c) in the right lung (×40). d and e), presence of SARS-CoV-2-infected cells in areas of the AFOP-like lesion: hematoxylin and eosin stain (d), and IHC for SARS-CoV-2 nucleocapsid antigen (e) (×200). f and g) Presence of CMV-infected cells in areas of the AFOP-like lesion: hematoxylin and eosin stain (f), and IHC for CMV antigen (g) (×400). Detailed information about microscopes utilized is indicated in Supplementary Methods.

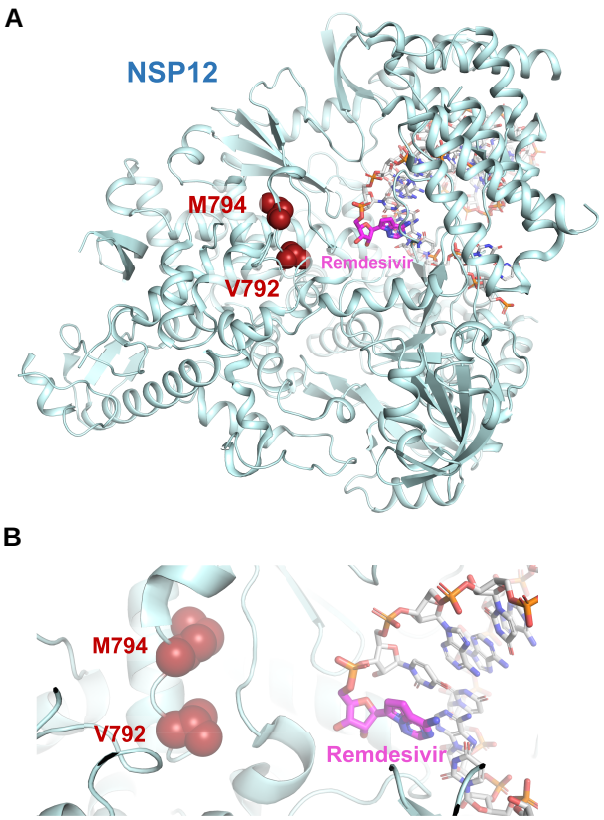

Fig. 3. Crystal structure of NSP12 of SARS-CoV-2 and remdesivir. A) The positional relationship between remdesivir and the residues of V792 and M794 on the crystal structure of NSP12. B) Close-up view of the mutation positions V792I and M794I in NSP12. The structure of the NSP12–NSP7–NSP8 complex (PDB ID 7BV2 PMID: 32358203) is shown as a cartoon representation in cyan. The RNA structure is shown as a white stick representation, and the remdesivir residue is in magenta. The residues of V792 and M794 are shown as CPK representations in red. This figure was prepared using PyMOL (30) (http://www.pymol.org/pymol).

Discussion

The risk of prolonged and severe COVID-19 in patients with hematologic diseases has been previously reported. Dulery et al. (2) reported a high frequency of prolonged hospitalization in BCL cases, such as DLBCL, FL, and marginal zone lymphoma in 2020 before vaccination, was implemented, and a significant correlation between prolonged hospitalization and risk of death, especially with treatment that includes anti-CD20 antibodies and in relapse/refractory cases. Visco et al. (3) extracted the prognostic risk factors of COVID-19 in unvaccinated malignant lymphoma (ML) patients and showed that age 65 or higher, male sex, lymphopenia, and thrombocytopenia were significantly associated with risk of death. A retrospective analysis of breakthrough COVID-19 in hematologic disease cases after January 2021, after the start of vaccination, showed a 9% mortality rate 30 days after onset, a decrease compared with prevaccine data (4). On the other hand, it has also been reported that the acquisition of antispike antibodies after vaccination is extremely poor in patients with BCL and chronic lymphocytic leukemia who are treated with anti-CD20 antibodies and/or BTK inhibitors (22, 23, 32). Even now with significant uptake of vaccines, there is concern for severe and prolonged COVID-19 in patients receiving anti-CD20 antibody therapeutics.

Recently, a phenomenon has been observed in clinical settings where viral load is not reduced by various antiviral treatments, especially in patients who are undergoing or have recently completed treatment for ML. Prolonged infection (sometimes over 3–6 months) has been reported, especially in patients treated with both an anti-CD20 antibody and bendamustine (33–35). Bendamustine has the properties of both an alkylating agent and a purine analog (36) and is potent in eliminating lymphocytes. In particular, it has been shown that it may take >2 years for the CD4-positive T-cell count to normalize after the last dose (37). In addition, elevated exhaustion markers have been observed in CD4-positive T cells in cases of prolonged infection (33). Furthermore, a recent report indicates that CD4-positive T-cell counts trended lower in patients with prolonged viral shedding compared with those without (35). Based on these data, we speculate that the host factors driving persistent COVID-19 may include both B- and T-cell functions, particularly the number of CD4-positive T cells and their dysfunction. The three cases we reported in this study were all older than 65 years of age and were treated with a combination of an anti-CD20 antibody and bendamustine within 2 years of the onset of COVID-19, resulting in critically low CD4-positive T-cell count below 100 cells/μL at the time of infection. In such markedly immunosuppressed hosts, SARS-CoV-2 may not only be difficult to eliminate but may also be provided the time and place to survive and accumulate additional mutations during prolonged infection (5, 20).

In both of the two autopsy cases, we observed a variety of pathologies throughout the lungs, including fibrosis and alveolar hemorrhage, as previously reported (38, 39). Case 1 also showed hyaline membrane formation and alveolar epithelialization, suggesting that irreversible changes had progressed with protracted infection. In both cases, SARS-CoV-2 was still present in alveolar cells at the time of death. CMV overlap infection may be associated with poor prognosis (40, 41), a phenomenon that requires special attention in clinical practice. In particular, in case 1, coexistence of SARS-CoV-2/CMV in the same cell was confirmed for the first time. These findings underscore the importance of considering infectious diseases other than COVID-19 in the differential diagnoses, since severe immunodeficiency is assumed to exist in the background of cases with prolonged SARS-CoV-2 infection.

Viral genome sequences were compared to identify genetic mutations generated during the course of each case. Most notably, the mutations in the residues 790s in NSP12, either V792I or M794I, were observed across the three cases following remdesivir treatment (Fig. 1A–C). Previous studies have shown several mutation sites in NSP12 responsible for remdesivir resistance. To date, P323L, S759A, V792I, E796G, C799F/R, and E802D were identified by in vitro selection with remdesivir (24, 42), and V792I, C799F, and E802D were found from immunocompromised individuals with prolonged infection (20, 43). P323L is preserved in the variants of concern, including Omicron (44). In the present study, a potential candidate for remdesivir resistance, M794I, was detected in cases 1 and 3. Therefore, we here investigated characteristics of M794I mutation together with V792I as a known resistance mutation. By comparison of recombinant viruses with or without resistance mutations, M794I conferred reduced susceptibility to remdesivir comparable to V792I and an increase in EC_{50} by ~2.5- to 4.5-fold compared with WT (Fig. 4A). The replication efficiency in cultured cells was lower for the mutant viruses, especially V792I (Fig. 4B). In vivo, either of the mutations clearly reduced pathogenicity (Fig. 4C). Torii et al. also associated a recombinant virus bearing E796G/C799F with decreased pathogenicity in hamsters (24). These results suggest that remdesivir resistance mutations are detrimental to viability within the hosts in the absence of remdesivir. This is consistent with Focosi's

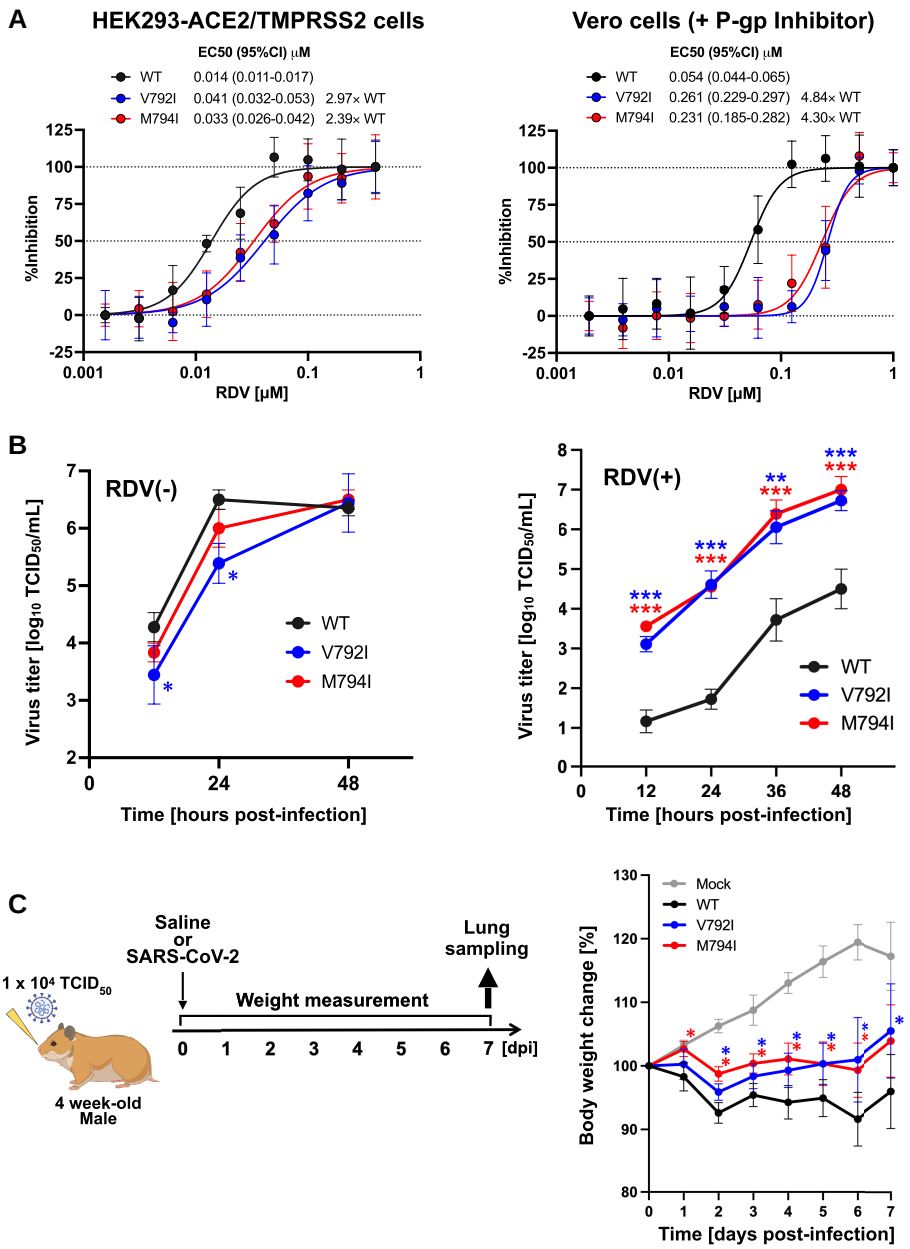

Fig. 4. Virological features of V792I and M794I mutants. A) Evaluation of remdesivir susceptibility using recombinant SARS-CoV-2 carrying the GFP gene. HEK293-ACE2/TMPRSS2 cells or VeroE6/TMPRSS2 cells treated with a P-gp inhibitor were infected with either WT, V792I, or M794I mutant at a MOI of 0.05 containing a 2-fold serial dilution of remdesivir. After 72 h in HEK293-ACE2/TMPRSS2 cells or 48 h in VeroE6/TMPRSS2 cells, the inhibition of infection was quantified via observation of GFP signals from four biological experiments, and then the EC_{50} of each virus was calculated by nonlinear regression analysis. B) Viral growth kinetics of WT, V792I, and M794I mutants using Vero cells in the absence (left panel) and presence (right panel) of remdesivir. Culture supernatants were collected at 12, 24, and 48 h postinfection, and infectious titers were determined and calculated as $TCID_{50}$/mL. C) Pathogenicity of the remdesivir-resistant viruses in Syrian hamsters. A group of 4-week-old hamsters ($n = 6$) were inoculated intranasally with either saline (uninfected control), WT, V792I, or M794I virus. The body weight was examined daily by 7 days postinfection. Data represent mean ± SD. Statistical analyses were performed using one-way ANOVA with multiple comparisons (the Dunnett's test) compared with WT as a control. Asterisks indicate significant differences (*$P < 0.05$, ** $P < 0.01$, *** $P < 0.001$).

report that showed the very low frequencies of viruses with remdesivir resistance in databases such as GISAID (45). We also gathered the full-length sequences registered in GISAID between June 2021and May 2023 (from Alpha wave to the early Omicron wave) and found that the frequency of V792I and M794I was still quite rare, although it tended to increase to over 0.01% of the total after the Omicron era (Fig. S5). These findings imply that there is a high barrier to transmission even if resistant viruses are continuously shed from individuals with prolonged infection. In the in vivo analysis using hamsters, while the difference in reactivity to remdesivir between WT and mutated viruses was suggested by weight change, we were unable to confirm a significant difference in virus amount in each lung after remdesivir treatment (Figs. 4 and S4). This suggests the need to consider the systemic effects of mutant SARS-CoV-2, as well as the need for further consideration of the duration of remdesivir administration and timing of analysis. Analysis strategies in vivo are considered an issue for future study.

Sequence analysis of the specimens of case 1 identified two mutations in the spike gene that have been associated with resistance to sotrovimab, namely E340A and E340D, and another novel change (F342INS). Substitution of E340 with other amino acids has been reported to confer resistance to sotrovimab (29, 46). Regarding abnormalities like F342INS, we speculate that F342INS may compromise the antibody binding and cause resistance since N343 is glycosylated and the monoclonal antibody reportedly recognizes the glycan (Fig. S2) (47). In case 1, a mutation in NSP5 (C10560G) resulting in T169S was also detected (data not shown). Considering a recent report correlating the T169 mutation (48) indicating the correlation with nirmatrelvir resistance, there is a possibility that this mutation contributes to nirmatrelvir resistance. Since this mutation is consistently detected regardless of the use of nirmatrelvir, it is suggested that this is not a mutation acquired after the use of nirmatrelvir.

Interestingly, at least two major substrains were present in the patient between the onset and 15 weeks in case 1, and appeared in the nasopharyngeal swab specimens in turns (Fig. 1A). After the first remdesivir treatment, the substrain with E340A gained V792I in the NSP12 (second sample). Then with the second remdesivir treatment M794I appeared in NSP12 possibly in both of the substrains (E340A + M794I in the eighth collection and F342INS + M794I in the eleventh sample), but the V792I and M794I substitutions seem mutually exclusive. Furthermore, additional mutations accumulated suddenly after the twelfth sample, which may be attributed to treatment with molnupiravir known to cause random errors of sequence fidelity during viral genome replication by acting as an analogue of cytosine or partially uracil (49).

All patients we described in this study were markedly immunodeficient, influenced by the primary disease, and immunochemotherapy. We speculate that suboptimal anti-SARS-CoV-2 antibody generation following vaccination among patients undergoing B-cell depletion therapy by anti-CD20 antibodies, in addition to poor recovery of CD4-positive T cells over a long period of time with bendamustine, made containment of infection difficult. In the fatal cases, lack of SARS-CoV-2-specific immune response despite vaccination, resistance to antiviral therapies, and superinfection by other viral and bacterial pathogens together contributed to progressive tissue injuries and irreversible multiple organ failure. Considering treatment of ML in the COVID-19 era, it may be important to select a treatment regimen that limits the dysfunctional state of the lymphocytes to as short periods as possible. Since recent reports have also shown that T cells involved in antiviral activity are induced by vaccination even among patients who do not develop antibodies (50), it is important to administer updated boosters as appropriate. Prophylactic administration of anti-SARS-CoV-2 antibody products is also considered (8). Finally, the development of new strategies that differ from those of healthy individuals, such as combination treatment with antiviral drugs (51) that may substantially reduce viral load in the early stages of disease onset to prevent the virus from having the opportunity to acquire resistance mutations, will be an important consideration.

Acknowledgments

The authors thank Yuko Sato and Seiya Ozono (Department of Pathology, National Institute of Infectious Diseases), and H. Maruyama and M. Hanazaki (Department of Microbiology and Immunology, Faculty of Medicine, Hokkaido University) for technical assistance. The authors thank all the hospital staff involved in the COVID-19 care and all the caregivers, including the patients' families.

Supplementary Material

Supplementary material is available at *PNAS Nexus* online.

Funding

The authors declare no funding.

Author Contribution

C.I., T.Ic., Y.D., T.F., T.M., and A.T. designed the study. C.I., T.Ic., T.Ta., M.T., T.Is., M.Ib., R.K., M.Iw., and A.T. treated the patients and collected patients' samples and clinical data. T.Tsuk., Y.I., T.Tsuj., Y.O., S.T., N.O., Y.K., and S.N. performed the pathological diagnosis. T.S., Y.H., S.I., and H.K. performed the pathological and genetic analysis using tissue sample. T.Ta., M.S., H.A., N.N., and H.S. performed the sequencing analysis. A.Kaw. performed the protein structural analysis. T.Ic. performed the drug susceptibility analysis. A.Kam. and T.Ta. performed the animal experiments. C.I., T.Ic., and A.T. wrote the main manuscript text and prepared tables and figures. Y.D., T.F., T.M., and A.T. supervised the study and critically reviewed. All authors participated in discussions and interpretation of the data and results.

Data Availability

The RNAseq data of case 1 specimens 1 to 12 in Fig. 1A will be available from NCBI SRA (PRJNA1049969). The data of case 1 specimen 13 in Figs. 1A and S2 (at autopsy) will be available from DDBJ DRA (DRA017735). The sequence data of cases 2 and 3 are available from DDBJ (accession numbers: case 2: LC798944, LC753061, and LC753062; case 3: LC798945, LC798946, and LC798947).

References

1 Zsichla L, Muller V. 2023. Risk factors of severe COVID-19: a review of host, viral and environmental factors. *Viruses*. 15(1):175.
2 Dulery R, *et al.* 2021. Prolonged in-hospital stay and higher mortality after COVID-19 among patients with non-Hodgkin lymphoma treated with B-cell depleting immunotherapy. *Am J Hematol*. 96(8):934–944.
3 Visco C, *et al.* 2022. A prognostic model for patients with lymphoma and COVID-19: a multicentre cohort study. *Blood Adv*. 6(1):327–338.
4 Pagano L, *et al.* 2022. Breakthrough COVID-19 in vaccinated patients with hematologic malignancies: results from the EPICOVIDEHA survey. *Blood*. 140(26):2773–2787.
5 DeWolf S, *et al.* 2022. SARS-CoV-2 in immunocompromised individuals. *Immunity*. 55(10):1779–1798.
6 Gupta A, *et al.* 2021. Early treatment for COVID-19 with SARS-CoV-2 neutralizing antibody sotrovimab. *N Engl J Med*. 385(21):1941–1950.
7 Weinreich DM, *et al.* 2021. REGN-COV2, a neutralizing antibody cocktail, in outpatients with COVID-19. *N Engl J Med*. 384(3):238–251.
8 Levin MJ, et al. 2022. Intramuscular AZD7442 (tixagevimab-cilgavimab) for prevention of COVID-19. *N Engl J Med*. 386(23): 2188–2200.
9 Beigel JH, *et al.* 2020. Remdesivir for the treatment of COVID-19. *Final Report. N Engl J Med*. 383(19):1813–1826.

10 Rueda JC, *et al.* 2022. Can presence of HLA type I and II alleles be associated with clinical spectrum of CHIKV infection? *Transbound Emerg Dis*. 69(4):e895–e905.
11 Hammond J, *et al.* 2022. Oral nirmatrelvir for high-risk, nonhospitalized adults with COVID-19. *N Engl J Med*. 386(15):1397–1408.
12 Polack FP, *et al.* 2020. Safety and efficacy of the BNT162b2 mRNA COVID-19 vaccine. *N Engl J Med*. 383(27):2603–2615.
13 Baden LR, *et al.* 2021. Efficacy and safety of the mRNA-1273 SARS-CoV-2 vaccine. *N Engl J Med*. 384(5):403–416.
14 Tuekprakhon A, *et al.* 2022. Antibody escape of SARS-CoV-2 Omicron BA.4 and BA.5 from vaccine and BA.1 serum. *Cell*. 185(14):2422–2433.e2413.
15 Wang Q, *et al.* 2022. Antibody evasion by SARS-CoV-2 Omicron subvariants BA.2.12.1, BA.4 and BA.5. *Nature*. 608(7923):603–608.
16 Imai M, *et al.* 2023. Efficacy of antiviral agents against Omicron subvariants BQ.1.1 and XBB. *N Engl J Med*. 388(1):89–91.
17 Takashita E, *et al.* 2022. Efficacy of antibodies and antiviral drugs against COVID-19 Omicron variant. *N Engl J Med*. 386(10):995–998.
18 Miller J, *et al.* 2023. Substantial neutralization escape by SARS-CoV-2 Omicron variants BQ.1.1 and XBB.1. *N Engl J Med*. 388(7):662–664.
19 Jackson CB, Farzan M, Chen B, Choe H. 2022. Mechanisms of SARS-CoV-2 entry into cells. *Nat Rev Mol Cell Biol*. 23(1):3–20.
20 Gandhi S, *et al.* 2022. De novo emergence of a remdesivir resistance mutation during treatment of persistent SARS-CoV-2 infection in an immunocompromised patient: a case report. *Nat Commun*. 13(1):1547.
21 Awadasseid A, Wu Y, Tanaka Y, Zhang W. 2021. Effective drugs used to combat SARS-CoV-2 infection and the current status of vaccines. *Biomed Pharmacother*. 137:111330.
22 Okamoto A, *et al.* 2022. CD19-positive lymphocyte count is critical for acquisition of anti-SARS-CoV-2 IgG after vaccination in B-cell lymphoma. *Blood Adv*. 6(11):3230–3233.
23 Perry C, *et al.* 2021. Efficacy of the BNT162b2 mRNA COVID-19 vaccine in patients with B-cell non-Hodgkin lymphoma. *Blood Adv*. 5(16):3053–3061.
24 Torii S, *et al.* 2023. Increased flexibility of the SARS-CoV-2 RNA-binding site causes resistance to remdesivir. *PLoS Pathog*. 19(3):e1011231.
25 Torii S, *et al.* 2021. Establishment of a reverse genetics system for SARS-CoV-2 using circular polymerase extension reaction. *Cell Rep*. 35(3):109014.
26 Tomiyama T, *et al.* 2023. A third dose of the BNT162b2 mRNA vaccine sufficiently improves the neutralizing activity against SARS-CoV-2 variants in liver transplant recipients. *Front Cell Infect Microbiol*. 13:1197349.
27 Matsuyama S, *et al.* 2020. Enhanced isolation of SARS-CoV-2 by TMPRSS2-expressing cells. *Proc Natl Acad Sci U S A*. 117(13): 7001–7003.
28 Motozono C, *et al.* 2021. SARS-CoV-2 spike L452R variant evades cellular immunity and increases infectivity. *Cell Host Microbe*. 29(7):1124–1136.e1111.
29 Rockett R, *et al.* 2022. Resistance mutations in SARS-CoV-2 Delta variant after sotrovimab use. *N Engl J Med*. 386(15):1477–1479.
30 Mooers BHM. 2020. Shortcuts for faster image creation in PyMOL. *Protein Sci*. 29(1):268–276.
31 De Rosa MF, Sillence D, Ackerley C, Lingwood C. 2004. Role of multiple drug resistance protein 1 in neutral but not acidic glycosphingolipid biosynthesis. *J Biol Chem*. 279(9):7867–7876.
32 Tsutsumi Y, Ito S, Horikita F, Moriki A, Teshima T. 2023. COVID-19 antibody production by vaccination in chemotherapy with CD20 antibody for B-cell lymphoma. *Mol Clin Oncol*. 19(6):96.
33 Ikeda D, *et al.* 2023. Clinical and immunological characteristics of prolonged SARS-CoV-2 Omicron infection in hematologic disease. *Blood Cancer J*. 13(1):133.
34 Franceschini E, *et al.* 2023. Persistent SARS-CoV-2 infection with multiple clinical relapses in two patients with follicular lymphoma treated with bendamustine and obinutuzumab or rituximab. *Infection*. 51(5):1577–1581.
35 Ichikawa T, *et al.* 2023. Prolonged shedding of viable SARS-CoV-2 in immunocompromised patients with haematological malignancies: a prospective study. *Br J Haematol*. 204:815–820.
36 Hiraoka N, *et al.* 2014. Purine analog-like properties of bendamustine underlie rapid activation of DNA damage response and synergistic effects with pyrimidine analogues in lymphoid malignancies. *PLoS One*. 9(3):e90675.
37 Martinez-Calle N, *et al.* 2019. Kinetics of T-cell subset reconstitution following treatment with bendamustine and rituximab for low-grade lymphoproliferative disease: a population-based analysis. *Br J Haematol*. 184(6):957–968.
38 Flaifel A, *et al.* 2022. Pulmonary pathology of end-stage COVID-19 disease in explanted lungs and outcomes after lung transplantation. *Am J Clin Pathol*. 157(6):908–926.
39 Li Y, *et al.* 2021. Progression to fibrosing diffuse alveolar damage in a series of 30 minimally invasive autopsies with COVID-19 pneumonia in Wuhan, China. *Histopathology*. 78(4):542–555.
40 Krivosikova L, *et al.* 2023. Long COVID complicated by fatal cytomegalovirus and Aspergillus infection of the lungs: an autopsy case report. *Viruses*. 15(9):1810.
41 Mangieri CW, *et al.* 2023. Switching perfusion agents for repeat cytoreductive surgery with hyperthermic intraperitoneal chemotherapy: surgical dogma or evidence-based practice? *Ann Surg Oncol*. 30(1):384–391.
42 Stevens LJ, *et al.* 2022. Mutations in the SARS-CoV-2 RNA-dependent RNA polymerase confer resistance to remdesivir by distinct mechanisms. *Sci Transl Med*. 14(656):eabo0718.
43 Hogan AB, *et al.* 2023. Estimating long-term vaccine effectiveness against SARS-CoV-2 variants: a model-based approach. *Nat Commun*. 14(1):4325.
44 Vangeel L, *et al.* 2022. Remdesivir, molnupiravir and nirmatrelvir remain active against SARS-CoV-2 Omicron and other variants of concern. *Antiviral Res*. 198:105252.
45 Focosi D, Maggi F, McConnell S, Casadevall A. 2022. Very low levels of remdesivir resistance in SARS-COV-2 genomes after 18 months of massive usage during the COVID19 pandemic: a GISAID exploratory analysis. *Antiviral Res*. 198:105247.
46 Huygens S, Oude Munnink B, Gharbharan A, Koopmans M, Rijnders B. 2023. Sotrovimab resistance and viral persistence after treatment of immunocompromised patients infected with the severe acute respiratory syndrome coronavirus 2 Omicron variant. *Clin Infect Dis*. 76(3):e507–e509.
47 Pinto D, *et al.* 2020. Cross-neutralization of SARS-CoV-2 by a human monoclonal SARS-CoV antibody. *Nature*. 583(7815):290–295.
48 Nooruzzaman M, *et al.* 2024. Emergence of transmissible SARS-CoV-2 variants with decreased sensitivity to antivirals in immunocompromised patients with persistent infections. *Nat Commun*. 15(1):7999.
49 Kabinger F, *et al.* 2021. Mechanism of molnupiravir-induced SARS-CoV-2 mutagenesis. *Nat Struct Mol Biol*. 28(9):740–746.
50 Atanackovic D, *et al.* 2022. T cell responses against SARS-CoV-2 and its Omicron variant in a patient with B cell lymphoma after multiple doses of a COVID-19 mRNA vaccine. *J Immunother Cancer*. 10(7):e004953.
51 Orth HM, *et al.* 2023. Early combination therapy of COVID-19 in high-risk patients. *Infection*. 52(3):877–889.